AIAA Aviation
16-20 June 2014, Atlanta, GA
44th AIAA Fluid Dynamics Conference

Vortex-Array Model of a Shear Layer Perturbed by a Periodically Pitching Airfoil

K. Zhang [1]
Xi'an Jiaotong University, Xi'an, China

A.M. Naguib[2] and M.M. Koochesfahani[3]
Michigan State University, East Lansing, MI-44824, USA

The unsteady flow in the wake of a harmonically pitching airfoil placed at the center of a two-stream shear layer is investigated. The chord Reynolds number of the airfoil is approximately 12,000, based on the average velocity of the two streams, and the shear-layer Reynolds number is 1150/cm. Single-component Laser Doppler Velocimetry measurements are used to examine the transverse profiles of the streamwise velocity, averaged at different phases of the oscillation cycle, in the wake of the airfoil and their relation to the underlying flow features observed from flow visualization. The outcome of this analysis is employed as basis for constructing a structure-based model for computation of the velocity across the wake. The model consists of an array of Gaussian-core vortices whose circulation, core size, and spatial location are varied to provide the best reproduction of the experimentally measured velocity. The results show that the model provides good agreement with the experiments overall. However, additional tuning of some of the model details is necessary to remedy the remaining discrepancies between the model calculations and the experiments.

Nomenclature

c	=	airfoil chord
f	=	frequency (Hz)
i,j	=	summation indices
k	=	reduced frequency
L_x	=	streamwise length of the vortex-array model
N	=	number of large-scale vortices in the vortex array model
n	=	number of small-scale vortices in the vortex array model
$R_{o,v}$	=	core radius of the large-scale vortices in the vortex-array model
$R_{o,vs}$	=	core radius of the small-scale vortices in the vortex-array model
r	=	ratio of the low- to the high-speed-stream streamwise velocity $r = U_2/U_1$
$r_{i,v}$	=	radial coordinate measured from the center of the ith large-scale vortex in the vortex-array model
$r_{j,v}$	=	radial coordinate measured from the center of the jth small-scale vortex in the vortex-array model
U	=	time-average streamwise vleocity
U_o	=	mean streamwise velocity of the low- and the high-speed streams
U_1	=	high-speed stream velocity
U_2	=	low-speed stream velocity
u	=	streamwise velocity
$\langle u \rangle$	=	phase-averaged streamwise velocity
u_{rms}	=	root mean square of the streamwise velocity
v	=	transverse velocity
v_{rms}	=	root mean square of the transverse velocity
X	=	streamwise coordinate
$X_{ci,v}$	=	streamwise coordinate of the core center of the ith large-scale vortex in the vortex-array model

[1] Lecturer, State Key Laboratory for Strength and Vibration of Mechanical Structures, School of Aerospace.
[2] Professor, Department of Mechanical Engineering, AIAA Associate Fellow.
[3] Professor, Department of Mechanical Engineering, AIAA Associate Fellow.

$X_{cj,vs}$	=	streamwise coordinate of the core center of the jth small-scale vortex in the vortex-array model
X_m	=	streamwise coordinate of the measurements
Y	=	transverse coordinate
$Y_{ci,v}$	=	transverse coordinate of the core center of the ith large-scale vortex in the vortex-array model
$Y_{cj,vs}$	=	transverse coordinate of the core center of the jth small-scale vortex in the vortex-array model
Y_{max}	=	transverse coordinate of the maximum transverse gradient of the streamwise velocity
Y_o	=	transverse coordinate of the location where $U = U_o$
α	=	angle of attack
α_o	=	angle of attack amplitude of oscillation
β	=	inclination angle of the linear vortex sheet relative to the X direction in the vortex-array model
ΔU	=	difference between the low- and high-speed stream velocities
Φ	=	oscillation cycle phase relative to the airfoil motion ($\Phi = 0$ corresponds to $\alpha = 0$ at pitch-up)
$\Gamma_{o,v}$	=	circulation of the large-scale vortices in the vortex-array model
$\Gamma_{o,vs}$	=	circulation of the small-scale vortices in the vortex-array model
λ	=	wavelength (corresponding to streamwise spacing between successive large-sale vortices)
θ	=	momentum thickness of the shear layer
Ψ	=	oscillation cycle phase relative to the large-scale vortex ($\Psi = 0$ corresponds to vortex located at X_m)

I. Introduction

RECENTLY, the study of low-Reynolds number unsteady aerodynamics has received heightened attention because of interest in unmanned micro air vehicles (UMAVs) based on the flapping wing concept (e.g. Wilson[1], Lai and Platzer[2]). The behavior of flow around airfoils executing highly unsteady motion has been studied for decades. However, understanding the underlying fluid mechanical phenomena, predictive capabilities, and experimental data remain insufficient regarding the fundamental unsteady aerodynamics of low Reynolds number MAVs[3]. Experimental and computational studies[2,4,5] have demonstrated that the wake of a periodically pitching airfoil is characterized by concentrated vortices, and the pattern of the vortex structures varies with the motion parameters (amplitude, frequency, waveform, etc.). The force acting on the airfoil changes with the wake vortex pattern. For example, a net thrust force can be established on the airfoil when the wake vortex pattern is opposite to that of the traditional Kármán vortex street. Recently, Naguib *et al.*[6] employed a simple, vortex-array model of the wake vortex pattern to compute the unsteady velocity field in the wake of a periodically pitching airfoil embedded in a uniform flow. The model predictions agreed well with experimental data of the streamwise velocity in the wake of an oscillating NACA 0012 airfoil embedded in uniform freestream. The model was also successful in estimating the mean thrust acting on the airfoil.

Most of the investigations on low-Reynolds number unsteady aerodynamics has focused on the unsteady flow around a pitching and/or plunging airfoil embedded in a uniform approach flow. However, in real life, MAVs could experience a variety of complicating factors such as wind gusts, turbulence and wind shear. Flapping-wing flight provides MAVs the potential of better tolerance to wind gusts and flow disturbances[3]. An important component in developing such tolerance capability is to understand how the flow around the airfoil is altered due to the presence of unsteadiness and non-uniformities in the freestream. To this end, the present work is motivated by studying the influence of unsteady shear in the approach flow on the vortical structures and associated unsteady streamwise velocity in the wake of a periodically pitching airfoil. The specific flow configuration examined is that of an airfoil embedded in a two-stream shear layer. The focus of the analysis is on relatively low reduced frequency of oscillation and in the far wake where the flow is predominantly that of the shear layer, perturbed by the presence of the oscillating airfoil.

The data employed in the present study represent a subset of those discussed in an earlier study by Koochesfahani and Dimotakis[7]. Koochesfahani and Dimotakis[7] presented results concerning the shear-layer statistics only, whereas in this work the unsteady streamwise velocity field in the wake of the pitching airfoil will be investigated. In addition, the feasibility of modeling the flow downstream of the airfoil using a simple vortex-array model, based on ideas similar to those of Naguib *et al.*[6] will be studied. Such physics-based, low-order models could be useful for: (I) interpreting observations of the velocity field and forces acting on the airfoil in terms of the underlying flow features and their characteristics; (II) complementing single-point measurements to extract flow structure information; (III) computing of the mean drag/thrust acting on the airfoil efficiently.

II. Experiment

Details of the experimental data have been reported elsewhere (Koochesfahani and Dimotakis[7]). Essential information is briefly described here for completeness. The experiment is conducted in a low-speed water tunnel. A two-dimensional shear-layer flow with a velocity ratio, $r = U_2/U_1$, of approximately 0.44 is produced downstream of a splitter plate in the water tunnel. The flow velocity of the high-speed stream, U_1, is 20.6 cm/s, resulting in a Reynolds number based on $\Delta U = U_1 - U_2$, of about 1150/cm. A NACA 0012 airfoil with chord c = 8 cm and extending across the span of the water tunnel is pitched about the ¼-chord point in the center of the shear layer, as depicted schematically in Fig. 1. The pitch axis of the airfoil is placed 27 cm downstream of the trailing edge of the splitter plate, and at a transverse location where the mean velocity equals the average of the low- and high-speed stream velocities: $U_o = (U_1 + U_2)/2$. The chord Reynolds number based on U_o is approximately 12,000. The airfoil is pitched sinusoidaly with amplitude (α_o) of 4 degrees around a mean angle of attack of zero at three oscillation frequencies: f = 0.25, 0.347 and 0.5 Hz. The corresponding reduced frequency $k = \pi fc/U_o$ = 0.42, 0.59 and 0.84.

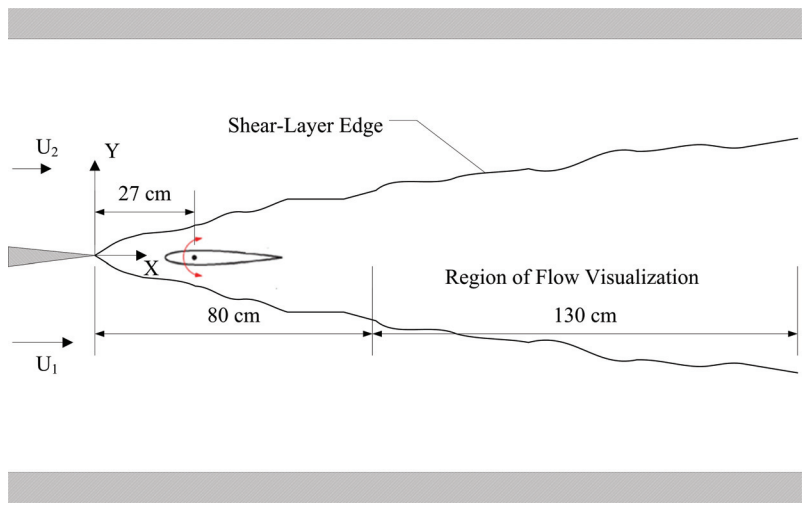

Figure 1. Sketch of the experimental configuration and employed coordinate system.

Measurement of the streamwise velocity is conducted using an LDV in the dual scatter mode at streamwise location X = 135 cm over a range $-0.15 < (Y-Y_o)/X < 0.15$ in the transverse direction, where Y_o is the Y coordinate of the position where the mean velocity is U_o. The angle of attack (α) of the airfoil is recorded simultaneously with the velocity using an optical encoder to enable calculation of phase-averaged quantities relative to the airfoil motion.

III. Experimental Results

Using the flow visualization images in Fig. 2, Koochesfahani and Dimotakis[7] showed the dramatic change of the flow structures and growth rate of the shear layer downstream of the airfoil when it is pitching periodically. Organized vortex structures roll up in the wake of the oscillating airfoil as a result of forcing the shear layer. The pattern of the vortex structures is quite different from that when the airfoil is oscillating in a uniform approach flow at similar reduced frequency, where the Kármán vortex street, or a modulated version of it, is observed. The size of the vortex structures and their wavelength (streamwise separation between two successive vortices) depicted in Fig. 2 increases as the oscillation frequency decreases. This is consistent with the cross-stream profiles of the mean and the root means square (rms) streamwise velocity in Fig. 3. The figure shows the extent of the cross-stream region of mean shear to increase, and the corresponding maximum velocity gradient to decrease, with decreasing forcing frequency. The rms fluctuations also extend over a wider cross-stream domain with decreasing forcing frequency. Both of these effects appear to be manifestations of the increasing scale of the shear-layer vortices with decreasing forcing frequency.

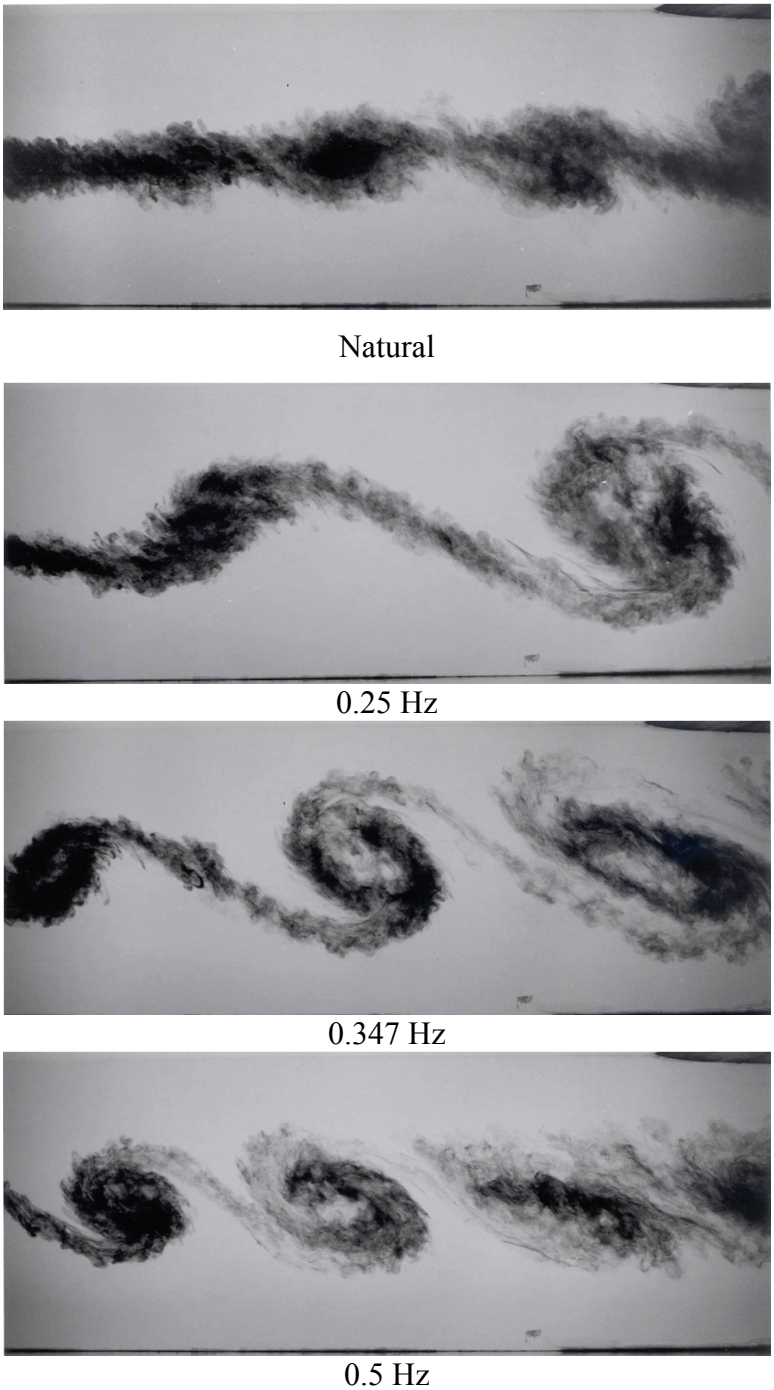

Figure 2. Dye flow Visualization from Koochesfahani and Dimotakis[7] showing the shear-layer vortical structures downstream of the airfoil for different oscillation frequencies (flow is from left to right). The field of view of the images is as noted in Fig. 1.

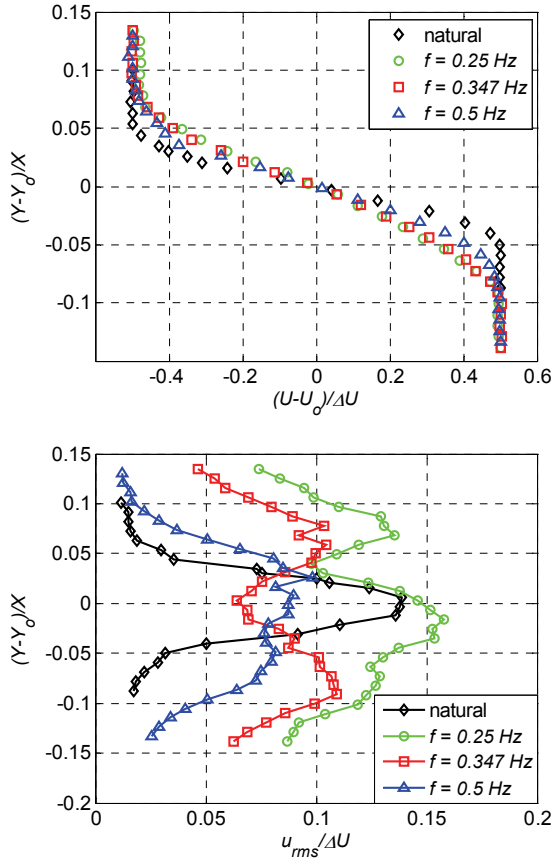

Figure 3. Mean and rms streamwise-velocity profiles at X = 135 cm

Phase-averaged streamwise velocity profiles are shown in Fig. 4. In order to obtain these profiles, the oscillation cycle is subdivided into 50 equal, non-overlapping, intervals spanning from the beginning of the oscillation cycle (corresponding to airfoil angle of attack of 0 degrees during the pitch-up phase), designated as $\Phi = 0$, to the end of the cycle, designated as $\Phi = 1$. The streamwise-velocity data are sorted into these intervals, or phase bins, based on the simultaneously recorded angle of attack information, and data falling into the same phase bin are averaged to get the phase-averaged velocity. Figure 4 displays the phase-averaged streamwise velocity profile at eight different phases of the oscillation cycle: Φ = 0, 0.12, 0.25, 0.375, 0.5, 0.625, 0.75 and 0.875 for f = 0.25 Hz (the only frequency of oscillation considered hereafter). The red lines superposed on the profile correspond to boundaries of the "high-shear" region where the velocity gradient $d\langle u\rangle/dY$ is within 50% of the maximum value.

The velocity profiles in Fig. 4 show that the high-shear region is concentrated in a relatively narrow zone over a good portion of the oscillation cycle. This zone, marked by a pair of red lines, seems to shift progressively in the positive cross-stream direction with increasing time (as shown by the arrow on top of the figure) from below, at Φ =0.75, to above the shear-layer centerline. In the remainder of the oscillation cycle, the high-shear region widens to eventually encompass most of the measurement domain. An explanation of this behavior can be reached by inspection of the underlying flow structure, seen in the flow visualization picture placed beneath the phase-averaged velocity profiles in Fig. 4. The picture clearly depicts two vortical structures, forming from the roll-up of the shear layer in response to the airfoil oscillation. The two vortical structures, which are expected to produce a shear region spanning a domain of the same size as the vortex, are connected with a "braid" that is much smaller in cross-stream scale and is inclined at an angle relative to the streamwise direction. As the braid convects past the X location of the measurements, one would expect it to produce a narrow zone of high shear that progressively moves in the upward direction with increasing time due to the inclination of the braid. As the upstream end of the braid travels past the measurement location, the measured shear zone is anticipated to gradually increase in cross-stream scale, eventually spanning the full shear-layer width, as the braid is followed by a large-scale vortex. These observations are consistent with the characteristics of the phase-averaged velocity profiles discussed earlier.

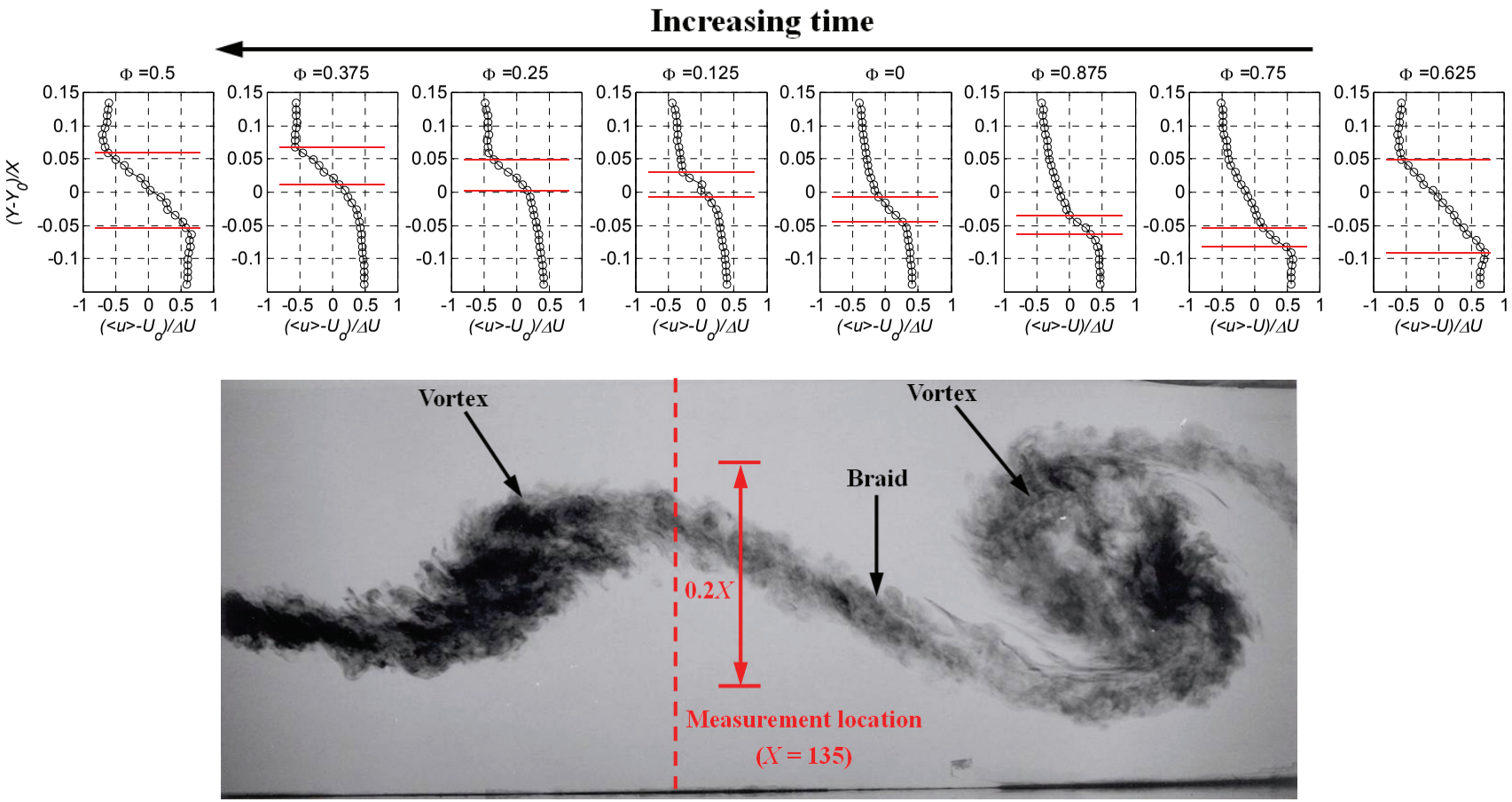

Figure 4. Streamwise-velocity profiles obtained from an average at selected phases of the oscillation cycle for f = 0.25 Hz (top), and flow visualization image depicting the corresponding flow structure (bottom). Φ = 0 corresponds to an airfoil angle of attack of zero during pitch up.

IV. The Vortex-Array Model

A vortex-array model based on ideas similar to those employed in Naguib *et al.*[6] is utilized to represent the shear layer flow in the wake of the oscillating airfoil. The model is constructed by prescribing a streamwise-periodic spatial distribution of vorticity that is consistent with the flow features discussed in the previous section. Thus, one wavelength λ of the prescribed vorticity field is composed of one large-scale vortex and a number of smaller vortices representing the braid, or "vortex sheet", which "connects" the large vortex structures, as illustrated in Fig. 5. All vortices are assumed to have a core with Gaussian vorticity distribution with the circulation of the vortices representing the vortex sheet given by $\Gamma_{o,vs}$, and that of the large-scale vortex is $\Gamma_{o,v}$. The corresponding core radii are $R_{o,vs}$ and $R_{o,v}$, respectively, with the latter being appreciably larger than the former.

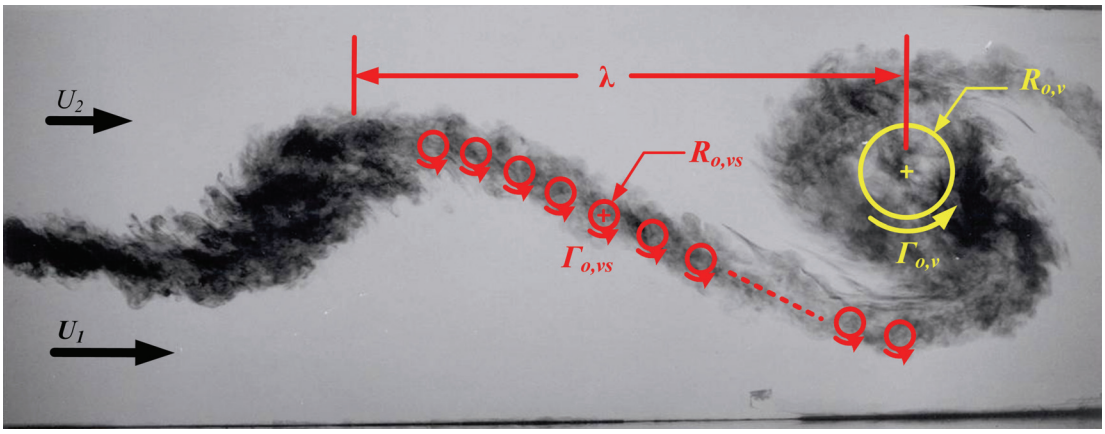

Figure 5. Illustration of the arrangement of the Guassian-core vortices used to model the braid (red) and large-scale vortex (yellow) over one wavelength λ in the vortex-array model of the perturbed shear layer in the wake of the airfoil.

The final vorticity distribution of the model is obtained by repeating the vortex-array configuration shown in Fig. 5 N times in the streamwise direction with a wavelength $\lambda = U_o/f$ to mimic the periodic shear-layer vortex structure. Unlike the actual flow, however, where the circulation and scale of the large-scale vortices and the braid characteristics change in the streamwise direction, the characteristics of the vortex array shown in Fig. 5 are selected to match the vorticity characteristics at the measurement location, but then kept unchanged when periodically extending the array. This is done for simplicity and with the expectation that variation in the vorticity distribution within wavelengths other than the one containing the calculation location will cause minimal difference in the computed velocity. Specifically, the velocity is calculated from the prescribed vorticity distribution using the Biot-Savart law. Based on the latter, it can be shown that the difference between the actual and "frozen" vorticity distribution within wavelengths other than that containing the calculation location relate to the dipole and higher-order poles of the vortex pattern in these "distant" wavelengths. The corresponding "induced" velocity decays at least quadratically with distance, and hence these differences should have minimal, if any, influence on the computed velocity.

Using the Biot-Savart law, it can be shown that the streamwise (u) and transverse (v) components of the velocity induced at a point (X,Y) by the vortex array, including N+1 large vortices (one is added because an extra large vortex is employed at the most upstream end of the model) and $n\times N$ small vortices representing the vortex sheet, superposed onto a uniform flow with a streamwise velocity of U_o is given by:

$$u(X,Y) = U_0 - \sum_{i=1}^{N+1} \frac{\Gamma_{i,v}(r_{i,v})}{2\pi} \frac{(Y - Y_{ci,v})}{r_{i,v}^2} - \sum_{j=1}^{nN} \frac{\Gamma_{j,vs}(r_{j,vs})}{2\pi} \frac{(Y - Y_{cj,vs})}{r_{j,vs}^2} \tag{1}$$

$$v(X,Y)=\sum_{i=1}^{N+1}\frac{\Gamma_{i,v}(r_{i,v})}{2\pi}\frac{(X-X_{ci,v})}{r_{i,v}^2}+\sum_{j=1}^{nN}\frac{\Gamma_{j,vs}(r_{j,vs})}{2\pi}\frac{(X-X_{cj,vs})}{r_{j,vs}^2} \tag{2}$$

with,

$$\begin{aligned}\Gamma_{i,v}(r_{i,v})&=\Gamma_{o,v}[1-e^{-(r_{i,v}/R_{o,v})^2}]\\ \Gamma_{j,vs}(r_{j,vs})&=\Gamma_{o,vs}[1-e^{-(r_{j,vs}/R_{o,vs})^2}]\end{aligned} \tag{3}$$

In Eq. (1) to Eq. (3), $(X_{ci,v},Y_{ci,v})$ is the coordinate of the center of the ith large-scale vortex, and $(X_{cj,vs}, Y_{cj,vs})$ is the coordinate of the center of the jth small vortex along the vortex sheet, and $r_{i,v}$ and $r_{j,vs}$ are the radial coordinates measured from the center of the ith large-scale vortex and the jth small vortex, respectively, to point (X,Y).

As a starting point, the small vortices representing the vortex sheet are distributed equally-spaced along a straight line ('linear vortex sheet') that is inclined with an angle β to the X direction while being tangent to circles representing the upstream and downstream large-scale vortex core (see Fig. 6). The centerline of the large-scale vortex is set at $Y = Y_o$, which causes the center point of the vortex sheet to be located at the centerline as well. The overall configuration of the entire vortex array is given in Fig. 6. The X location of the computation, which is the same as the measurement location (X_m), is taken to coincide with the core center of the large vortex at $t = 0$. The velocity is computed over the transverse coordinate range $(Y-Y_o)/X$ = -0.3 to 0.3 at 100 different time steps per oscillation cycle.

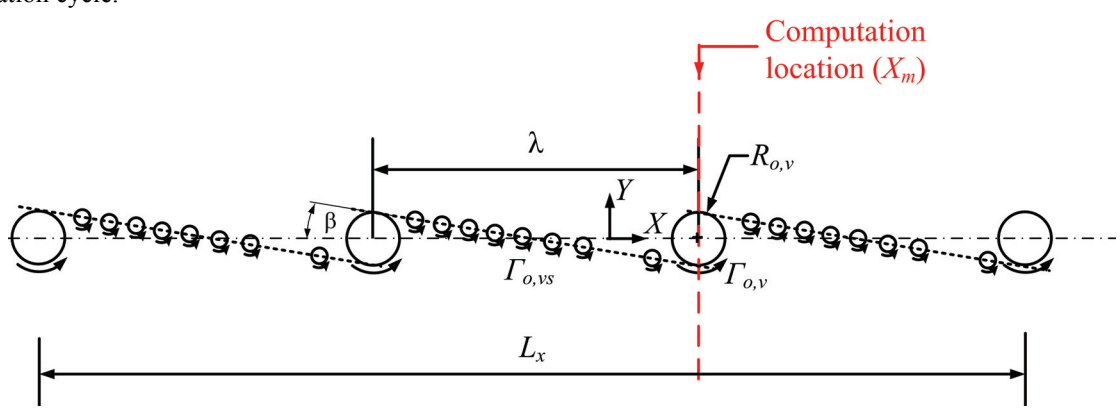

Figure 6. Configuration of the vortex-array-model representation of the perturbed shear layer in the wake of the oscillating airfoil for $N = 3$.

The model parameters, $\Gamma_{o,vs}$, $\Gamma_{o,v}$, $R_{o,vs}$ and $R_{o,v}$ are set by seeking the best match between the model prediction and the measurement of u at different phases of the oscillation cycle. In the present work, the "best match" is judged only qualitatively by visually inspecting comparisons between the computed and measured velocity profiles across the shear layer at several phases. The number of small vortices n in each wavelength, and the number of large vortices N +1(or the streamwise length of the model $L_x = N\lambda$) in the model is set based on the convergence of the velocity calculation. Figure 7 depicts the model predictions of the mean streamwise velocity $(U-U_0)/\Delta U$, the rms streamwise velocity $u_{rms}/\Delta U$ and the rms transverse velocity $v_{rms}/\Delta U$ for different n values while keeping N = 100. Figure 8 shows the same quantities but for different streamwise vortex-array lengths while keeping n =100: $L_x/\lambda = N$ = 10, 20, 50 and 100. Note that the cross-stream coordinate is normalized using the shear-layer momentum thickness θ, which will be used to non-dimensionalize all length scales in the remainder of the paper. For reference, the shear layer thickness is approximately 8θ. As seen in Fig. 7 and Fig. 8, it is difficult to discern any difference between the computed profiles when $n \geq 50$ and $L_x/\lambda \geq 50$. The model requires a relatively large number of vortices to converge (more than approximately 2500), but it only requires a few minutes to run when implemented in MATLAB on a PC.

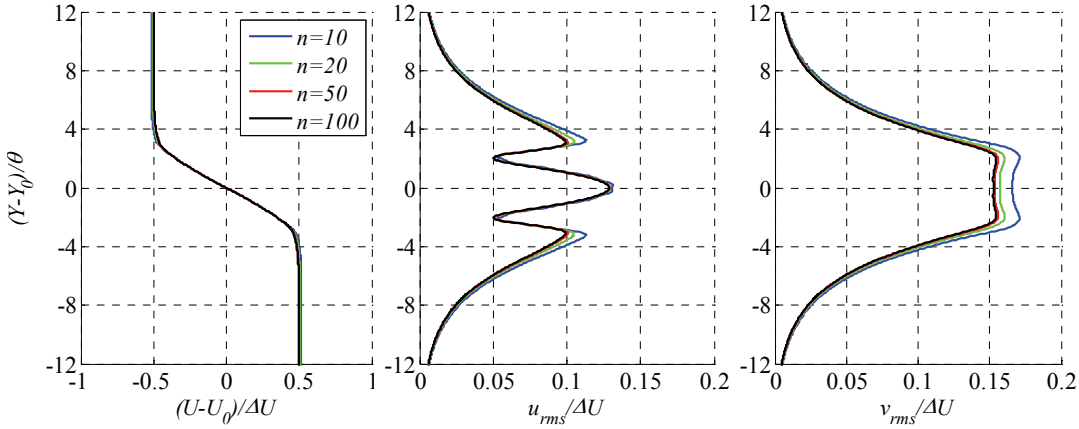

(a) (b) (c)

Figure 7. Dependence of the computed velocity profiles on *n* with *N* = 100: (a) mean streamwise velocity; (b) *rms* streamwise velocity; (c) *rms* transverse velocity.

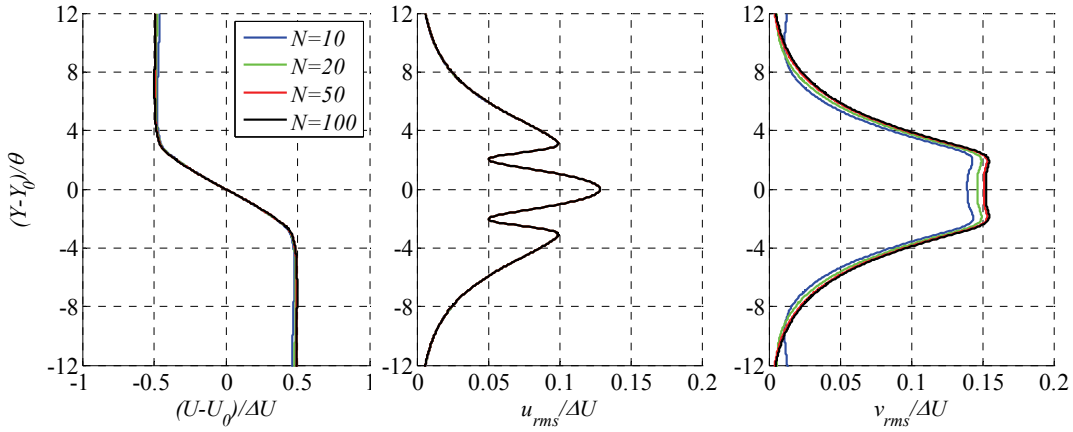

(a) (b) (c)

Figure 8. Dependence of the computed velocity profiles on *N* with *n* = 100: (a) mean streamwise velocity; (b) *rms* streamwise velocity; (c) *rms* transverse velocity.

The best prediction of the velocity profiles using the above vortex-array model, with the "linear vortex sheet", is compared against experimental data in Fig. 9. As seen in the figure, the model prediction of the mean streamwise velocity profile agrees well with the experimental data, while the calculated rms streamwise velocity is substantially lower than that obtained from the experiments. However, the shape of the computed rms velocity profile is qualitatively similar to the experimental counterpart, exhibiting three local peaks with the strongest one in the middle. The Y locations of the two weaker peaks in the computed profile agree well with the corresponding ones from the experiments. On the other hand, the middle, stronger, peak is found at Y_o in the computed profile, whereas the one observed experimentally is located below Y_o. Overall, the predicted rms profile is symmetric about Y_o, because of the symmetry of the model geometry with respect to Y, while the rms profile calculated from the experimental data exhibit some asymmetry about Y_o.

Examination of the phase-averaged velocity profile (not shown here for brevity) shows that there is discrepancy in the Y location of maximum shear (maximum $d\langle u\rangle/dY$) between the computation and measurement at several phases of the oscillation cycle. Thus, in an attempt to improve the vortex-array model prediction, the Y location of the centers of the small-scale vortices representing the vortex sheet is set such that the Y location of the vortex sheet at the computation location is the same as the Y location of the maximum shear (Y_{max}) observed experimentally at a given phase of the oscillation cycle. Note that Y_{max} is approximately the same as the location midway between the two red lines superposed on each of the phase-averaged velocity profiles in Fig. 4. Figure 10 shows Y_{max} versus phase, which is seen to move in the positive Y direction before dropping, fairly abruptly, at $\Phi = 0.45$ then rising up

again starting at $\Phi = 0.6$. By comparing with the underlying flow structure in the flow visualization in Fig. 4, the quick drop of Y_{max} from the highest to the lowest value is presumably associated with the passage of the large-vortex structure past X_m. Just downstream of the vortex, the braid is at its highest Y location, while just upstream of the vortex, the braid is at its lowest Y location; thus, the vortex passage leads to the quick change in Y_{max}. Consequently, the center of the large vortex structure is inferred to pass through X_m at $\Phi \approx 0.5$, and the gradually increasing Y_{max} value (notwithstanding some data scatter) from $\Phi \approx 0.05$ to 0.45 and $\Phi = 0.6$ to 0.95 corresponds to the passage of the center of the braid past the measurement location. For the purposes of the model, the Y_{max} variation with phase for the braid must be converted into variation with X to describe the locus along which the n small-scale vortices are placed. This is achieved by multiplying the time corresponding to a given phase by U_o (the convection velocity used in the model). The resulting locus of the vortex sheet is shown in Fig. 11, after shifting the phase such that the center of the large vortex is located at $X = 0$ (also at λ). In the modified model, the small vortices representing the vortex sheet are distributed equally-spaced (in X) along the locus shown in Fig. 11 over the domain $X/\lambda = 0.05 - 0.95$. No special provision is made to address some of the scatter observed in the experimentally determined locus (e.g. between $X/\lambda = 0.3 - 0.45$ and $0.65 - 0.85$). The overall configuration of the modified vortex-array model is shown in Fig. 12. The model also contains a new parameter b that allows imposition of a Y offset between the core center of the large vortex and Y_o.

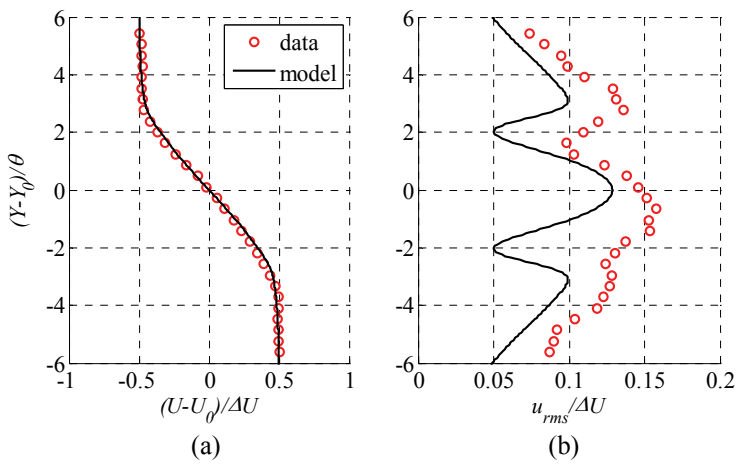

Figure 9. Comparison between the computed and measured velocity profiles: (a) mean streamwise velocity; (b) *rms* streamwise velocity. Model parameters are: $\Gamma_{o,vx}/\Delta U\theta$=0.075, $\Gamma_{o,v}/\Delta U\theta$= 10.2, $R_{o,vs}/\theta$ = 0.38, $R_{o,v}/\theta$ = 2.88, n = 100 and L_x/λ = 50.

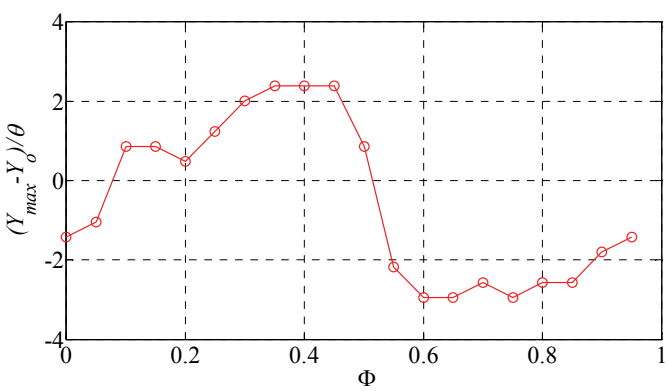

Figure 10. Measured Y location of the maximum shear versus phase of the oscillation cycle.

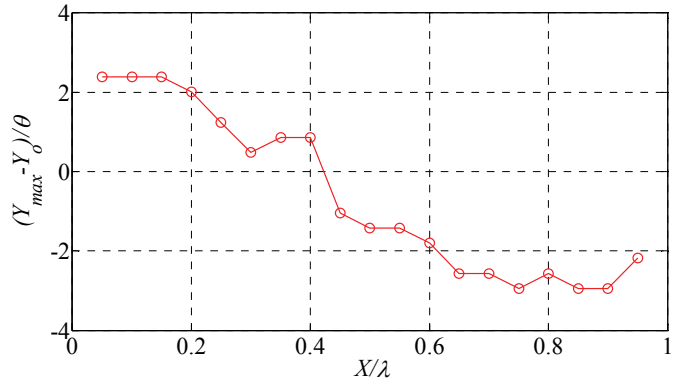

Figure11. Locus of the center of the vortex sheet in each wavelength of the modified vortex-array model.

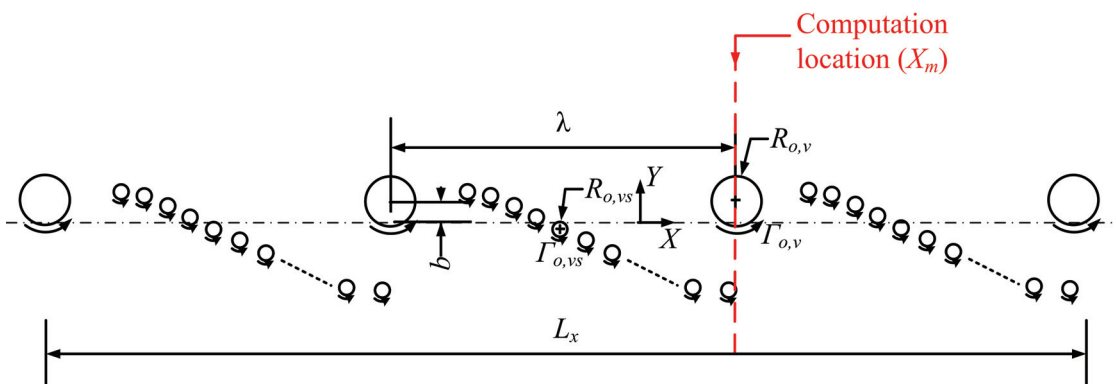

Figure 12. Configuration of the modified vortex-array-model representation of the perturbed shear layer in the wake of the oscillating airfoil for $N = 3$

V. Modeling Results

As discussed previously, the model parameters, $\Gamma_{o,vs}$, $\Gamma_{o,v}$, $R_{o,vs}$, $R_{o,v}$ and b are set by visually finding the best match between the model prediction and the measurement of u at selected phases of the oscillation cycle. Figure 13 displays the computed streamwise velocity profiles at eight different phases of the oscillation cycle Ψ = 0, 0.125, 0.25, 0.375, 0.5, 0.625, 0.75 and 0.875. The phase-averaged velocity at the same phases is also calculated from the experimental data and displayed in Fig. 13 using open circles. Note that Ψ is shifted by 0.5 relative to Φ (the oscillation cycle phase utilized hitherto) such that Ψ = 0 corresponds to the center of the core of the large-scale vortex coinciding with the calculation location. For reference, a schematic of the model vortex-array pattern relative to the computation location (X_m) is also given beneath the velocity profiles in Fig. 13 at Ψ = 0, 0.25, 0.5 and 0.75.

Overall, the results in Fig. 13 show that the model predictions agree well with the experimental data at most phases in the oscillation cycle, specially at $\Psi = 0$ when the large vortex passes through X_m. Some differences can be seen at different phases and and Y locations. For example, the computed velocity is higher than the measured value above Y_o at Ψ = 0.125, and the Y location of the maximum transverse velocity gradient, and the corresponding velocity profile slope, at Ψ = 0. 5 are different for the computed and measured profiles.

Additional comparison between the computed and measured velocity is given in Fig. 14 for the mean and rms velocity profiles. Note that no experimental data are shown for v_{rms} (Fig. 14c), since only the streamwise component of the velocity is measured. The computed results are shown though for reference and to highlight an advantage of the model in augmenting limited experimental data with additional information. As seen from Fig. 14, the model gives good prediction of the mean streamwise velocity. The "waviness" in the predicted mean velocity profile is a result of the unsmooth vortex sheet locus employed (Fig. 11). On the other hand, the computed rms streamwise velocity is lower than the experimental data at Y locations around $0 < (Y-Y_0)/\theta < 2$ and $(Y-Y_0)/\theta < -2$. However, the overall quantitative and qualitative agreement is better than that achieved using the linear-vortex-sheet model (Fig. 9). The above observations suggest that modeling of the vortex sheet require further improvement in order to arrive at more accurate predictions.

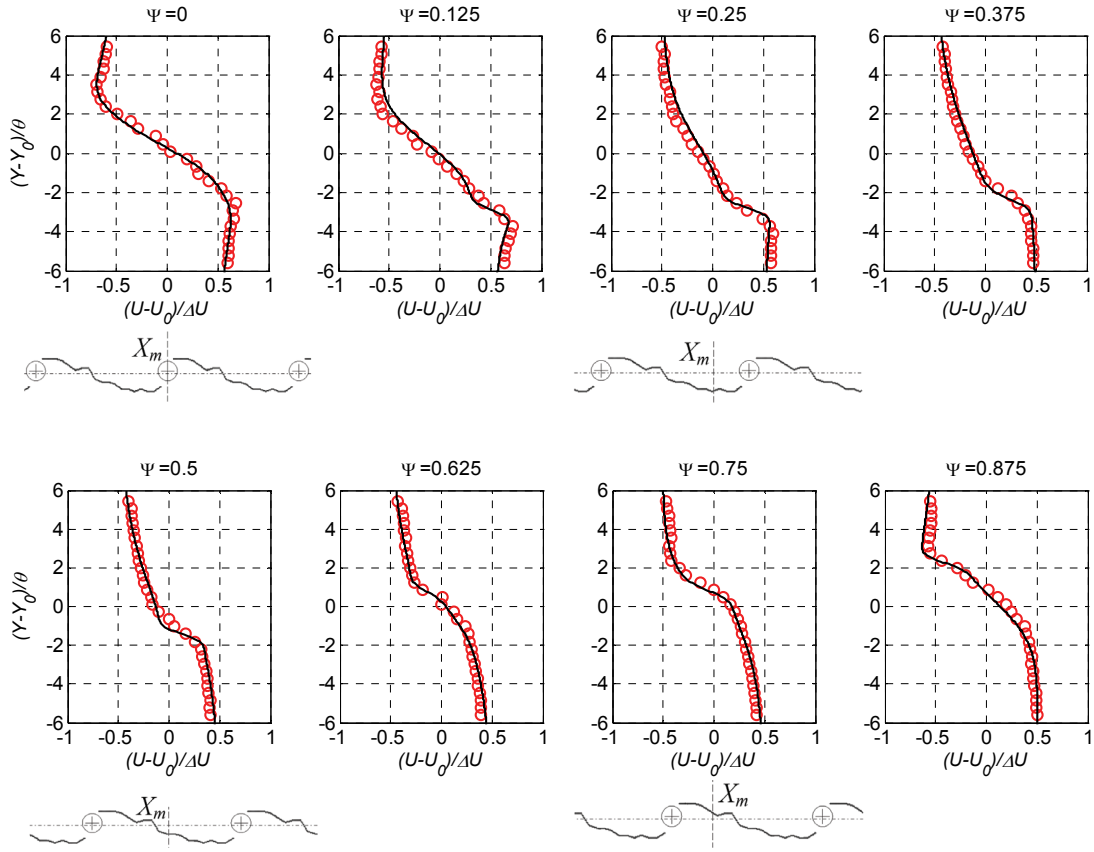

Figure 13. Comparison of the computed (line) and measured (symbols) streamwise velocity profiles at selected phases of the oscillation cycle. Model parameters are: $\Gamma_{o,vx}/\Delta U\theta$=0.04, $\Gamma_{o,v}/\Delta U\theta$= 10.8, $R_{o,vs}/\theta$ = 0.43, $R_{o,v}/\theta$ = 2.88, b/θ=0.36, n = 100 and L_x/λ = 50.

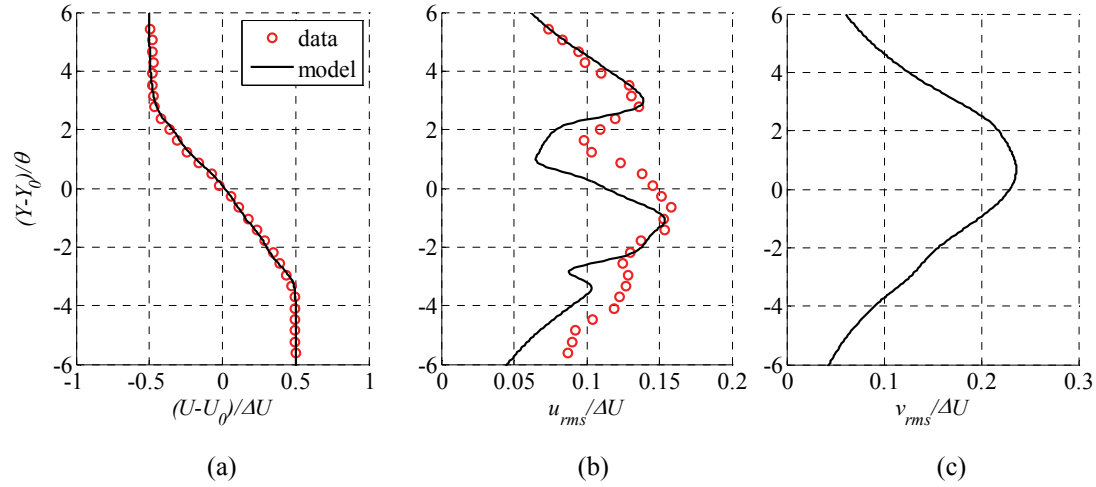

Figure 14. Comparison of the computed (line) and measured (symbols) streamwise velocity profiles: (a) mean streamwise velocity; (b) *rms* streamwise velocity; (c) *rms* transverse velocity. Model parameters are: $\Gamma_{o,vx}/\Delta U\theta$=0.04, $\Gamma_{o,v}/\Delta U\theta$= 10.8, $R_{o,vs}/\theta$ = 0.43, $R_{o,v}/\theta$ = 2.88, b/θ=0.36, n = 100 and L_x/λ = 50.

VI. Conclusion

In this paper, the unsteady velocity field in the wake of a harmonically pitching airfoil placed at the center of a two-stream shear layer is investigated. Measurements are used to obtain transverse profiles of the phase-averaged streamwise velocity at different phases of the oscillation cycle. The behavior of these profiles is interpreted in terms of the underlying shear-layer vorticity structure, inferred from flow visualization images. This leads to rationale basis for modeling the flow by using a Gaussian-core vortex-array to represent the large-scale shear-layer vortices and the braids that connect them. Overall, the model predictions agree well with the experimental data at different phases of the oscillation cycle. However, some quantitative discrepancies remain, and the results suggest that fine tuning the modeling details of the braid should lead to improvement in the model predictions.

Acknowledgments

The first author would like to acknowledge the support of her efforts by Chinese Fundamental Research Funds for the Central Universities 2011JDHZ22 and National Natural Science Foundation of China 11202157.

References

[1]Wilson, J. R., "Mini technologies for major impact," Aerospace America, May, 1998, pp. 36.

[2]Lai, J.C.S. and Platzer, M.F., "Jet characteristics of a plunging airfoil," *AIAA J.*, Vol. 37, No. 12, 1999, pp. 1529, 1537.

[3]Shyy, W., Lian, Y., Tang, J., Liu, H., Trizila, P., Stanford, B., Bernal, L., Cesnik, C., Friedmann, P, and Ifju, P., "Computational aerodynamics of low Reynolds number plunging, pitching and flexible wings for MAV applications," *AIAA Aerospace Sciences Meeting*, AIAA Paper No. AIAA-2008-523, January, 2008.

[4]Koochesfahani, M.M., "Vortical patterns in the wake of an oscillating airfoil," *AIAA J.*, Vol. 27, No. 9, 1989, pp. 1200, 1205.

[5]Anderson, J. M., Streitlien, K., Barrett, D. S. And Triantafyllou, M. S., "Oscillating foils of high propulsive efficiency," *J. Fluid Mech.*, Vol. 360, 1998, pp. 41, 72.

[6]Naguib, A.M., Vitek, J. and Koochesfahani, M.M., "Finite-core vortex array model of the wake of a periodically pitching airfoil," *AIAA J.*, Vol. 49, No. 7, 2011, pp. 1542, 1550.

[7]Koochesfahani, M. M. and Dimotakis, P. E., "Effects of a Downstream Disturbance on the Structure of a Turbulent Plane Mixing Layer," *AIAA J.*, Vol. 27, No. 2, 1989, pp. 161, 166.